Investigation of Failure Processes in Porous Battery Substrates: Part II—Simulation Results and Comparisons

X. Cheng

C. Wang

A. M. Sastry

S. B. Choi

Department of Mechanical Engineering,
and Applied Mechanics,
The University of Michigan,
Ann Arbor, MI 48109-2125

Models are presented for the evolution of transport and mechanical properties of nickel-metal hydride (NiMH) battery substrates. In the first paper in this series (Wang et al., 1999), conductive losses and enhancement of mechanical properties in these materials were quantified experimentally. These were qualitatively shown to be related to observed morphological changes in the substrate materials. Here, an evolution hypothesis for changes in these structures is presented, along with a simplified approximation of the real material microstructure (porous fiber/powder nickel network) with a tractable simulation geometry (porous fiber networks). Transport and mechanics models are then compared with experimental results, with stochastically-arranged fibers approximated as conductive beams connected by elastic torsion springs. Both quantitative and qualitative agreement are found with the models. Limitations of the approaches proposed are also discussed, along with the consequences of the simplifications of geometry for analysis.

I Introduction

Reduction of mass of substrate materials for us in NiMH cells offers great promise in producing higher energy densities in commercial cells, paving the way for more marketable electric vehicles and improved consumer electronics goods. The composition of these cells has been discussed in some detail in the first paper in this series, and in previous work by the authors (Sastry et al., 1998b; Wang et al., 1999a); briefly, porous substrates form a containment area and conductive grid for active material on the positive plate. Since these materials comprise a significant portion of the total cell weight, reduction of their overall mass is desirable, provided conductivity can be maintained in the cell over a long cycle life. Previous and ongoing analytical and numerical work has focused on development of models suitable to predict such behavior given detailed information about microstructure (on transport, Cheng et al., 1999a, b; on mechanics, Sastry et al., 1998a and Wang and Sastry, 1999).

Here, these models are refined for application to the observed evolving morphology of NiMH substrates during electrochemical cycling. A brief overview of previous work in modeling fibrous networks follows, with additional comments on the specific microstructures observed in NiMH batteries, and their evolution.

Previous Work: Percolation, Transport and Mechanics. There is a large body of literature in the percolation of low-density media, beginning Broadbent with Hammersley (1957) and later continued by, among others, Kirkpatrick (1973) and McLachlan (1988). In such problems, the critical parameter is the volume fraction of material (for a given microstructure) required to produce at least a single connecting path from one boundary to another, where the characteristic length of the problem domain scales with some characteristic length of the material microstructure. Fibrous materials have been specifically investigated by a number of workers, e.g., Pike and Seager (1973, 1974), Balberg et al. (1983). At the critical volume fraction, transport properties, including electrical conduction, rise dramatically. Previous efforts, elucidated some specific results for percolation of select geometries. Here, however, we attempt to provide quantitative linkage between material properties, variability, and microstructure.

The mechanics of fibrous materials (notably, by Cox, 1952; Hearle and Stevenson, 1964; and Lu et al., 1995, 1996a, 1996b) have also been studied, along with determination of the bounds on properties of such materials (e.g., Ostoja-Starzewski et al., 1989, 1990; Alzebdah et al., 1993; Borcea et al., 1997). Previous workers similarly have provided excellent frameworks for beginning analysis of such materials, but without the specificity needed in the current case. Particularly, work on development of bounds in material behavior has lacked ability to incorporate observed deformation mechanisms in realistic stochastic fibrous materials, and determine sufficiently narrow ranges of properties to be technologically useful in design of battery materials.

Motivation: Design of Substrate Materials, and Modeling Requirements. Design of superior electrode materials requires low-cost processing, low density construction, and high surface area/volume for the electrochemical reaction. Though random fiber architectures can fulfill these criteria, several questions have persisted concerning their design, e.g., what are the effects of staple length, aspect ratio and orientation in the fibers? To answer these questions, models must allow examination of the effects of details of microstructure. This need has motivated studies by the current authors, wherein generalized transport problems were compared to results of stochastic networks (Cheng et al., 1999a). These, in turn, were compared with full-field finite element solutions, wherein development of singularities in solution was also investigated (Cheng et al., 1999b).

In these previous studies, fiber staple length, orientation and aspect ratio at a full range of volume fractions were used to predict material conductivity. The present authors have also investigated the mechanics of stochastically-arranged fibers, using both rigidly-connected beam elements (Sastry et al., 1998b), and elastic response and failure of networks comprised of beam elements joined by elastic (torsion) springs (Wang and Sastry, 1999). This series of studies has addressed generalized problems of conduction, defor-

Contributed by the Materials Division for publication in the JOURNAL OF ENGINEERING MATERIALS AND TECHNOLOGY. Manuscript received by the Materials Division February 17, 1999; revised manuscript received June 25, 1999. Guest Editors: Assimina A. Pelegri, Ann M. Sastry, and Robert Wetherhold.

mation and failure, for a wider range of material types. Here, these models are used in conjunction with detailed studies of material response, and with experimentally verified models for material evolution. Such coupled experimental/theoretical analysis is critical in these low-density materials, since model predictions are dramatically affected by scale. Thus, specific information about microstructure has been used to generate numerical models for study, and scale effects have been investigated separately for the transport and mechanics problems.

II Development of Models and Simulations

Importantly, material microstructure is investigated in the geometry to which it is constrained in the cell ("compressed" condition), but also in the condition to which it evolves after electrochemical cycling ("post-cycled" condition). This allows comparisons of model predictions to experimental results for at least two states, for each material type.

Evolution Hypothesis. These comparisons require both general microstructural models for the different states of the material, along with an implicit hypothesis for the evolution of the material microstructure during cycling. Substrate materials in the as-received condition (described in detail in Wang et al., 1999) are of somewhat different morphology than model materials studied in generalized percolation problems. In typical percolation problems, conductive particles are assumed to be present in the problem domain by being fixed in a less- or non-conductive "matrix." Thus, particles are not necessarily connected to a structure with at least one single, domain-spanning, continuous path.

The materials investigated here, by contrast, are comprised only of conductive particles and fibers. Materials 1, 2, and 3 had volume fractions of 18%, 7%, and 5% conductive nickel, respectively, and were each comprised of a 50/50 blend of particles and fibers. In such materials, particles and fibers necessarily form an interconnecting network, and so we generally consider the materials under investigation to have around, or greater than, percolation volume fractions (which can be verified, provided testing is carried out on sufficiently large domains). The modeling here required some simplification in order to avoid full-field finite element calculations, since the aim was to perform enough simulations to generate realistic variances in properties. As described earlier (Cheng et al., 1999a), the fiber/particulate materials studied were modeled simply as fibrous networks, admittedly introducing some error in estimation of percolated material, but greatly simplifying geometry for simulations. Thus, all of the conductive mass was assumed to be part of fibers with the same geometry as the fibers in the material. This approach was motivated by 1) the geometry of the particles, which were of similar diameter to the fibers, and 2) the difficulty of describing the fiber-particle contact microstructure accurately in 2D (where particles placed in the unit cell would necessarily "overlap" fibers, thus necessitating 2D, versus 1D, representation of the fibers) and the attendant concern of continuous correction for volume fraction, since a 2D simulation "slice" of the material would not contain perfectly bisected particles.

Upon cycling, materials were seen to have altered morphology due to corrosion and electrodeposition in the positive plate. In this process, the small spherical particles were observed to be re-deposited onto the main fiber networks, resulting in less-distinct branches of particles within the fiber networks, and effectively thicker fibers. Additionally, experimental results showed increases in both stiffness and strength upon cycling of fibrous substrates for cells are in the compressed condition. A concurrent increase in resistivity in these materials was also observed. Thus, the following simplified assumptions/approaches were precluded:

(1) Attribution of conductive losses in substrates to breakdown in connectivity of materials during cycling. Loss of connectivity (i.e., the sequential failure of bonds and fiber segments due to swelling of networks) would explain losses in conduction (i.e. increase in resistivity), but would also result in loss of stiffness and strength.

(2) Modeling substrate morphology change with only an increase in constituent fiber aspect ratio, due to corrosion/electrodeposition during cycling. Previous work (Sastry et al., 1998b) showed that use of higher aspect ratio fibers results generally in improved mechanical properties. This would entail modeling the uncycled materials and cycled materials respectively, as higher-aspect ratio (with all conductive mass distributed in fibers of the same geometry as the fibers in the material) and lower-aspect ratio (with aspect ratio of the constituent fibers halved, to represent the deposition of all particle mass onto the fiber network) networks. While this evolution results in reduced resistivity, assuming that point contacts provide similar electron transfer (conductive transfer), it similarly would result in losses in stiffness and strength.

Thus, results pointed to use of a model for the fiber-fiber bonds with the observed evolution from higher to lower aspect ratio fibers. While overall resistivity was not assumed to be affected strongly by bond "integrity" (i.e., the torsional stiffness or strength of a fiber-fiber bond, dependent upon the amount of material at the bond), mechanical properties of the networks strongly depended on the nature of the bond. Previously (Sastry et al., 1998b), results for a range of microstructures were generated for the mechanical properties of such networks, assuming that bonds were rigid. Here, a torsional spring constant is assigned to each fiber-fiber bond; fibers are thus modeled as Euler beams joined by torsion springs. The torsional stiffness of each intersection is adjusted to produce experimentally-obtained moduli in each case. Thus, the deposition of nickel onto the main network is assumed to strengthen fiber-fiber bonds, so that bonds become "stiffer" in the post-cycled condition. The points of contact thus are assumed to become more rigid as material is deposited on the fibers during cycling, which both follows from the observed microstructures, and from the observed material behavior.

Transport Modeling. Following the approach taken in previous studies by the authors, stochastic networks were constructed in four steps, resulting in periodic arrays of stochastically-arranged 1D fibers, producing point-bonded structures as shown in Figs. 1. Resistivity of these networks is then calculated directly, assuming that all fibers segments have identical resistivity, so that each has resistance

$$R_i = \frac{\rho_f L_i}{A_i} = \frac{L_i}{A_i k_f} \tag{1}$$

where

A_i. . .cross-sectional area of ith fiber segmens
L_i. . .length of ith fiber segment
ρ_f. . .resistivity of ith fiber segment
k_f. . .fiber material conductivity

This results in conversion of the stochastic arrays to analytically tractable series/parallel resistor networks (Figs. 1(a–e)).

Mechanics and Damage Modeling. The mechanics analysis follows from previous work where simulations on a range of materials were conducted for the case of Euler beams connected by rigid bonds; this work was recently expanded to include the effects described earlier, wherein the bonds are viewed as torsion spring joints between fiber segments (Wang and Sastry, 1999), by addition of two springs elements onto each Euler beam element. A model single beam with endpoints 1 and 2, can be described as being subjected to axial loads (tension-positive, denoted F_1 and F_2), shear loads (upward-positive, denoted S_1 and S_2), torsion

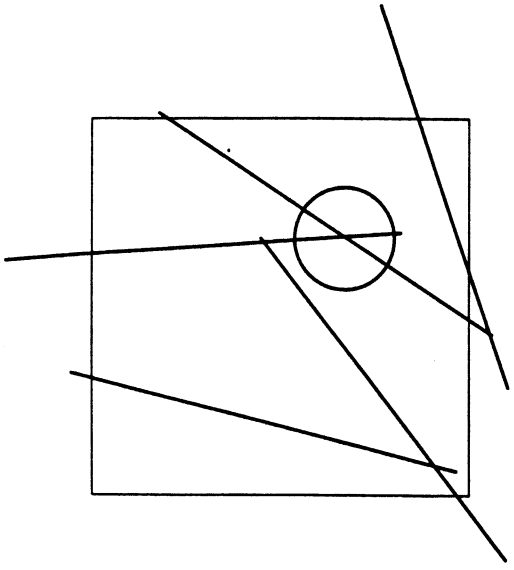

Fig. 1(*a*)

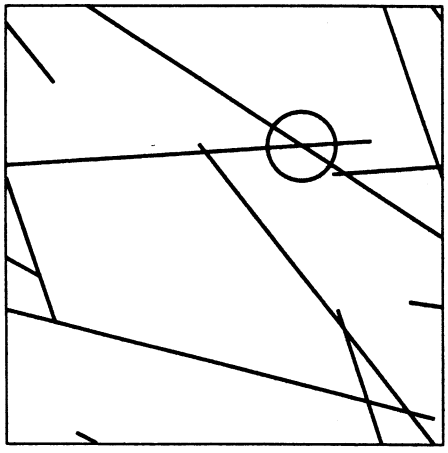

Fig. 1(*b*)

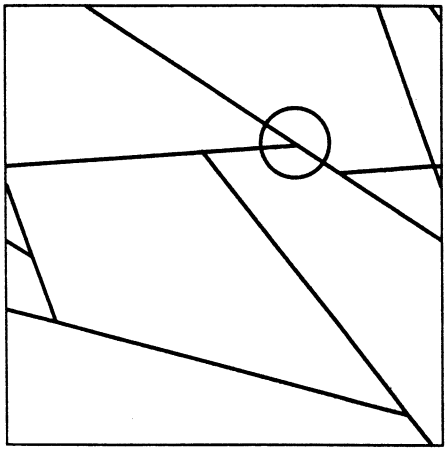

Fig. 1(*c*)

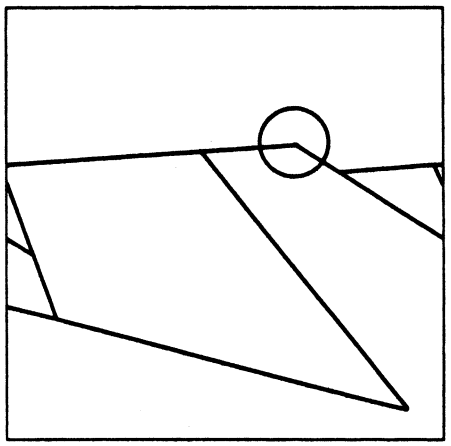

Fig. 1(*d*)

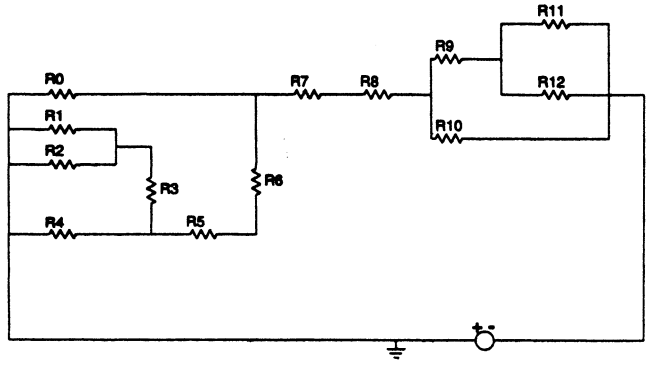

Fig. 1(*e*)

Fig. 1 Transport model for the porous fibrous network, where the original network generated numerically (*a*) is then converted to a periodic network (*b*). Extraneous "ends" are removed (*c*). A direction for current is then chosen (here, horizontal), which allows further reduction of the network (*d*), whereupon an equivalent resistor network can be generated for the array (*e*).

connection springs (with torsional spring constants K_{ts}) and moments (ccw-positive, denoted Q_1 and Q_2). The potential energy of this single beam, Π, can be written

$$\prod = \frac{1}{2}\int_0^L \left[EA\left(\frac{du}{dx}\right)^2 + EI\left(\frac{d^2v}{dx^2}\right)^2 \right] dx + \frac{1}{2}K_{ts}\left(\left.\frac{dv}{dx}\right|_{x=0} - \alpha_1\right)^2 + \frac{1}{2}K_{ts}\left(\left.\frac{dv}{dx}\right|_{x=L} - \alpha_2\right)^2 - Fu|_0^L - Sv|_0^L - Q\left.\frac{du}{dx}\right|_0^L \quad (2)$$

Minimization of potential energy results from solution of

$$\delta\prod = \int_0^L \left[EA\left(\frac{du}{dx}\right)\delta\left(\frac{du}{dx}\right) + EI\left(\frac{d^2v}{dx^2}\right)\delta\left(\frac{d^2v}{dx^2}\right) \right] dx + K_{ts}\left(\frac{dv}{dx_{x=0}} - \alpha_1\right)\delta\left(\left.\frac{dv}{dx}\right|_{x=0}\right) + K_{ts}\left(\frac{dv}{dx_{x=L}} - \alpha_2\right)\delta\left(\frac{dv}{dx_{x=L}}\right) - F\delta u|_0^L - S\delta v|_0^L - Q\delta\left.\frac{dv}{dx}\right|_0^L = 0 \quad (3)$$

Thus, the governing equations for this problem can be written as for an Euler beam, as

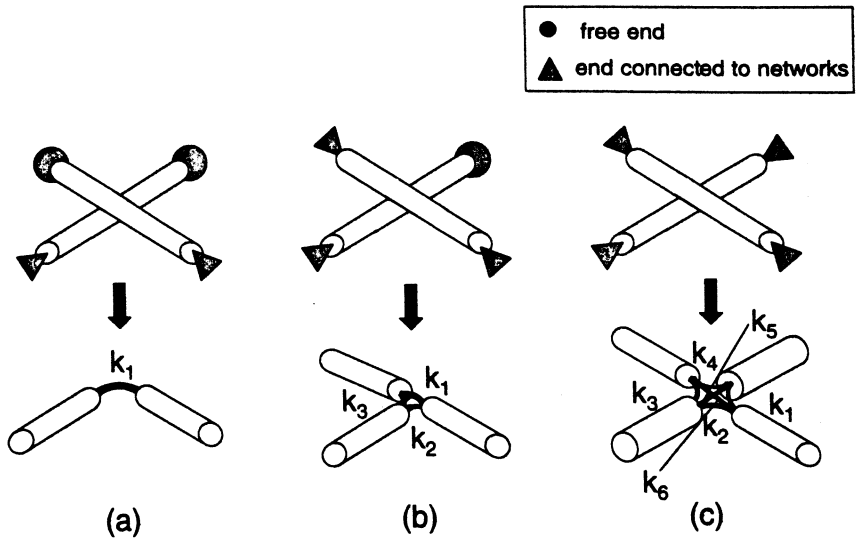

Fig. 2 Mechanics model for a torsion-spring bonded fibrous network, where beams (*a*) are used to model the segments, and fiber bonds are modeled as torsion springs. The torsion springs are assumed to have the same spring constant for two (*b*), three (*c*) or four (*d*) connected fibers at a single bond. Bonds (containing either two, three or four segments) are produced by "reductions" of the types as shown above each schematic.

$$EA\frac{d^2u}{dx^2} = 0$$

$$EI\frac{d^4v}{dx^4} = 0 \tag{4}$$

with boundary conditions given by

$$\left(EA\left(\frac{du}{dx}\right) - F_2\right)\delta(u)_{x=L} = 0$$

$$\left(-EA\left(\frac{du}{dx}\right) - F_1\right)\delta(u)_{x=0} = 0$$

$$\left(EI\left(\frac{d^2v}{dx^2}\right) - Q_2 + K_{ts}\frac{dv}{dx}_{x=L} - K_{ts}\alpha_2\right)\delta\left(\frac{dv}{dx}\right)_{x=L} = 0$$

$$\left(-EI\left(\frac{d^2v}{dx^2}\right) - Q_1 + K_{ts}\frac{dv}{dx}_{x=0} - K_{ts}\alpha_1\right)\delta\left(\frac{dv}{dx}\right)_{x=0} = 0$$

$$\left(-EI\left(\frac{d^3v}{dx^3}\right) - S_2\right)\delta(v)_{x=L} = 0$$

$$\left(EI\left(\frac{d^3v}{dx^3}\right) - S_1\right)\delta(v)_{x=0} = 0 \tag{5}$$

where angles $\alpha 1$, $\alpha 2$ are the angles formed by connection of the beam to other beams in the network.

Because of the technique for assembly of networks, via location of bonds at intersections of staple fibers, bonds generated fall into one of three categories, as shown in Figs. 2(*a–c*) (following from Fig. 1(*c*)). If two staple fibers intersect, but only two of the four ends remain after removal of free ends, situations such as Fig. 2(*a*) arise. Situations as in Figs. 2(*b*) and 2(*c*) arise from removal of a single free end, and removal of no free ends (i.e. all four "segments" are connected to the network after reduction), respectively. These situations are the only realistic outcomes, since fibers are modeled as 1D objects in calculation of intersections. More complicated intersections are possible when fibers are modeled as 2D objects.

This technique provides a simple means of extending previous work via addition of two energy terms for each beam element, however, it does contain the inherent difficulty of frequently treating continuous fibers as jointed segments, with considerably lower stiffness. This occurs in cases such as Figs. 2(*b*) and (*c*), where fibers spanning more than two joints are segmented. The effects of this assumption are described in detail in Wang and Sastry (1999).

The torsion springs at each joint are taken to be equal, i.e. separate springs were assigned to each connection, as in Figs. 2(*a–c*) with $k_1 = k_2 = \ldots = k_6$. The springs are not considered in the failure analysis; rather, the failure criteria were restricted to

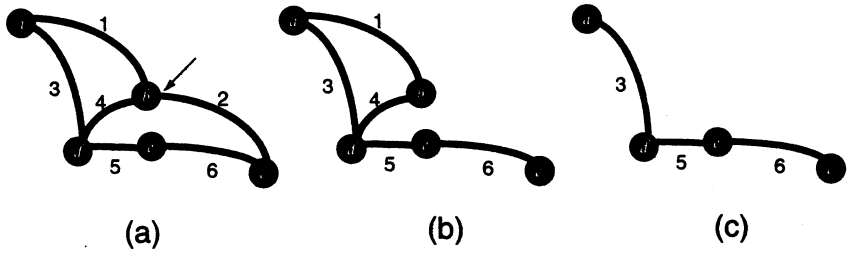

Fig. 3 Damage progression in the fibrous network. Two possible approaches are shown. The microstructure in (*a*), comprised of 6 fiber segments and 5 nodes (labeled) is deformed until a local failure initiates (arrow). The less conservative failure progression assumption (*b*) removes only fiber segment 2, since stress is maximized theoretically at its end at point *b*. The more conservative assumption is that the entire node *b* fails (*c*).

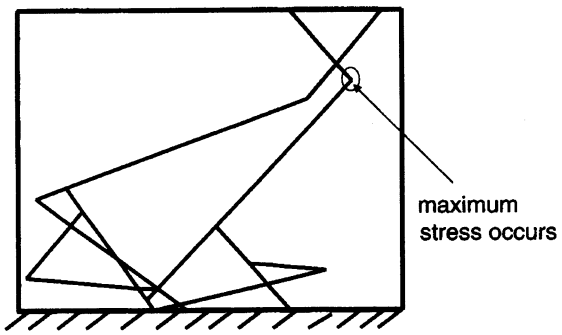

Fig. 4(*a*)

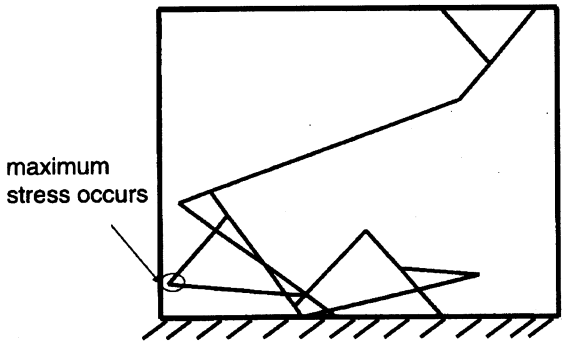

Fig. 4(*b*)

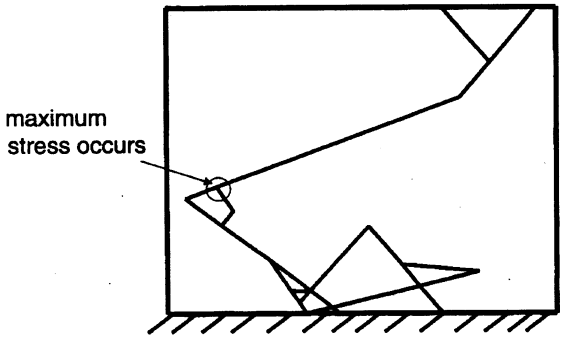

Fig. 4(*c*)

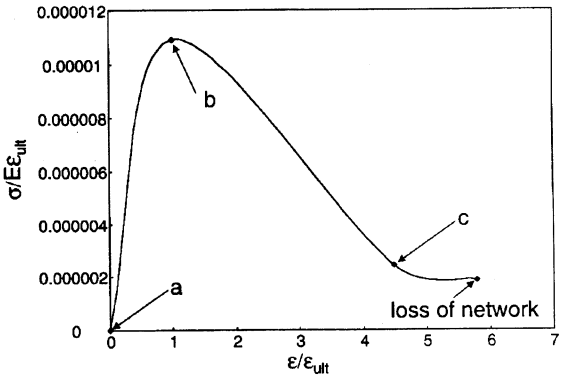

Fig. 4(*d*)

Fig. 4 Damage evolution in network simulations (actual case is shown, with original fibers' aspect ratio, *L*/*d* = 100, and original volume fraction of 6.28%). Uniaxial tension is applied to (*a*) the original network, whereupon the segment with the maximum load is failed, producing (*b*) the reduced network, after a single break. The simulation is continued, with further reductions in the network, producing (*c*) another reduction, until final failure (i.e. loss of the network) occurs. The resulting stress-strain curve for the simulation is shown in (*d*), where letters mark the stages corresponding to previous conditions.

analysis of the beams' ends, where stress was maximum. Two possible extreme cases could be considered in failure progression, as shown schematically in Figs. 3(*a–c*). In the first case, the maximum stress (located in the example at node *b* in beam 2) would cause failure only of segment 2. The more conservative approach was to consider the entire joint (and thus all connected beams) as failed for a segment failure. Investigation of the effects of these assumptions is described in other work, for rigid connections and for the case here (Wang and Sastry, 1999). The main difference is in the post-peak behavior for the two methods, with the assumption of sequential beam failure (Fig. 3(*b*)) resulting in more post-peak behavior than the sequential node failure (Fig. 3(*c*)). Moduli and strengths are similar for each approach. Figures 4(*a–c*) demonstrate the result of the beam failure approach for an actual network, with the final stress-strain curve shown in Fig. 4(*d*).

III Comparison of Models and Simulations

Simulations were run to compare the model compressed condition (identical to the as-received material except that the material was compressed to the same thickness as in the cell) and the model post-cycled condition (after which the material has undergone the morphological changes described earlier). Additionally, simulations were run in the transport simulations to assess scale effects. In the mechanics simulations, the simulation domains were approximately of the same order as the physical experiments.

Variation in staple length was also investigated in transport simulations. Material specifications included a range of staple lengths, so in the transport simulations, cases for each extreme were run and averaged. In the mechanics simulations, staple length was found to play an extremely strong role, especially in cases where the staple length was longer than the simulation domain length. This is discussed in greater detail in the following sections.

Table 1 Parameters used in transport simulations

material	volume fraction (%)	material condition	fiber diameter (μm)	staple length (cm)	simulation field size (cm)x(cm)
material 1	18%	as received	30	0.6	2.54 x 2.00 2.54 x 12.70
				1.35	2.54 x 2.00 2.54 x 12.70
	29.1%	compressed	30	0.6	2.54 x 2.54
				1.35	
		post-cycled	60	0.6	2.54 x 2.54
				1.35	
material 2	7.0%	as received	30	0.6	2.54 x 2.00 2.54 x 12.70 2.54 x 22.86
				1.35	2.54 x 2.00 2.54 x 12.70 2.54 x 22.86
	14.2%	compressed	30	0.6	2.54 x 2.54
				1.35	
		post-cycled	60	0.6	2.54 x 2.54
				1.35	
material 3	5.0%	as received	20	1.2	2.54 x 2.00 2.54 x 12.70 2.54 x 22.86
				2	2.54 x 2.00 2.54 x 12.70 2.54 x 22.86
	10.1%	compressed	20	1.2	2.54 x 2.54
				2	
		post-cycled	40	1.2	2.54 x 2.54
				2	

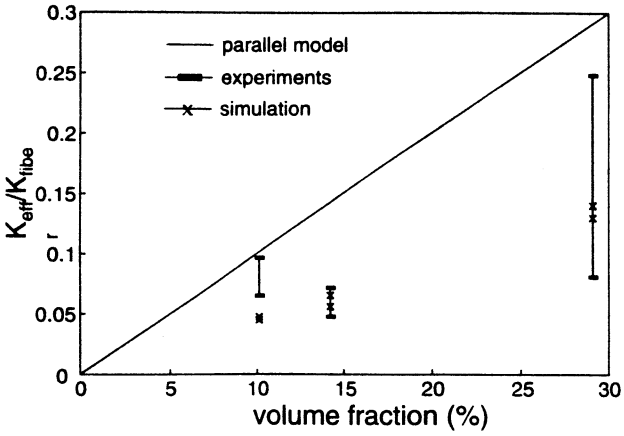

Fig. 5 Simulations versus experimental data. Resistivities of compressed materials versus upper bound predictions and simulation results, for each material type (10%, 14%, and 29% volume fractions).

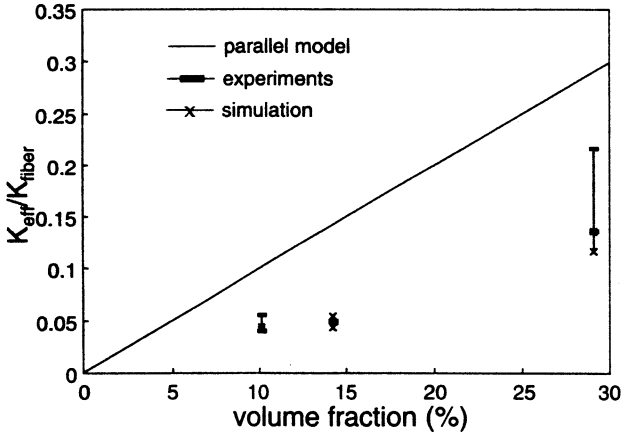

Fig. 6 Simulations versus experimental data. Resistivities of post-cycled materials versus upper bound predictions and simulation results, for each material type (10%, 14%, and 29% volume fractions).

Transport. A summary of the types of simulations performed is contained in Table 1. Volume fractions, fiber diameter, and range of staple lengths in each case were taken directly from manufacturer specifications (reported in Wang et al., 1999). Three "window sizes" were run for the as-received condition in all cases, to investigate scale effects in the transport simulations; in all cases, there was negligible effect in the range studied, so data reported represent averaged simulation results. Since detailed information about the distribution of staple lengths was not known, simulations in transport were run at each extreme of reported values, and similarly averaged, since staple length was not found to greatly affect results in transport.

Figures 5 and 6 show comparisons between simulation predictions including the upper bound (parallel model), on each plot, for reference; note that the lower bound, or series model, would produce zero conductivity in each case. Measurements were taken as described in Wang et al. (1999) for each condition, compressed (Fig. 5) and post-cycled (Fig. 6), respectively. Variances were higher for the experimental data in all cases than for the simulations.

In all cases, good agreement was obtained between simulations and experiments, with the low-density simulations providing the best agreement with experimental data. Particularly, the rigorous bounds provided extremely wide predictions in the resistivity of the materials, in addition to their inability to model differences between the resistivity of the morphologically altered materials (post-cycled versus compressed).

Mechanics/Damage. A summary of the types of simulations performed is provided in Table 2. These simulations were semi-empirical, in that torsion spring constants for each entire network were fitted to experimental data. This was done in order to allow some assessment of whether the effect of bond stiffness and strength played a role which could be reasonably supported by simulation. Simulations were performed for the same two material conditions, compressed and post-cycled. Simulation sizes were somewhat smaller than experimental test dimensions. Because mechanics simulations (unlike transport simulations) exhibited a very strong scale effect, the simulations were run using the shortest possible staple length in each case, so that the staple length/simulation window size was as small as possible. This is described in more detail later.

Figures 7(*a–f*) show comparisons of representative experimental curves with simulation curves (following the procedure outlined and described in Figs. 4(*a–d*)), for each material, in the compressed and post-cycled conditions. The failure stress was taken to be the fiber strength (543 MPa) in all cases, with fiber modulus taken as 210 GPa, for nickel substrate materials. The compressed cases showed higher compliance and lower strength for both experiments and simulation, and more brittle behavior than the post-cycled material.

Overall comparisons for the three material types are shown in Figs. 8–9 for moduli and Figs. 10–11 for the peak stresses, respectively, for all materials in the compressed and post-cycled conditions. The fitted torsion constants are shown Table 2. Torsion spring constants are normalized to (EI/l_s), where E is the fiber (nickel) modulus, I is the moment of inertia calculated for a cylindrical segment with diameter as shown, and l_s is the average segment length reported for each type of simulation [note that the average segment length was calculated for all networks in a category and used in reporting l_s]. Variances in experimental data, unlike those in measurement of resistivity, were lower than simulation variances in each case. Also, in most cases using the uniformly distributed staple length networks showed higher overall variances in mechanical properties.

Simulation results for peak stresses, despite the linearity of the model, were in reasonable agreement with the experimental data; in all cases, trends in simulations matched experimental trends.

Table 2 Parameters used in mechanics simulations

material	volume fraction (%)	material condition	fiber diameter (μm)	simulation field size (cm)x(cm)	staple length (cm)	average segment length (cm)	torsion spring (dimensionless, with $\frac{k_s}{EI/l_s}$)
material 1	29.10%	compressed	30	0.75x0.75	0.6	0.012	6.32e-05
		post- cycled	60	0.75x0.75	0.6	0.023	8.58e-03
material 2	14.20%	compressed	30	1.00x1.00	0.6	0.025	4.21e-03
		post-cycled	60	1.00x1.00	0.6	0.046	6.45e-01
material 3	10.10%	compressed	20	1.80x1.80	1.2	0.024	2.24e-04
		post-cycled	40	1.80x1.80	1.2	0.046	1.13e-02

Fiber strength: 542.5MPa; Young's modulus: 210GPa

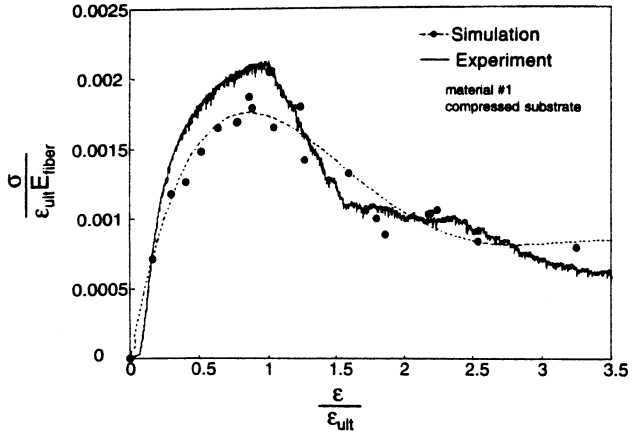

Fig. 7(*a*)

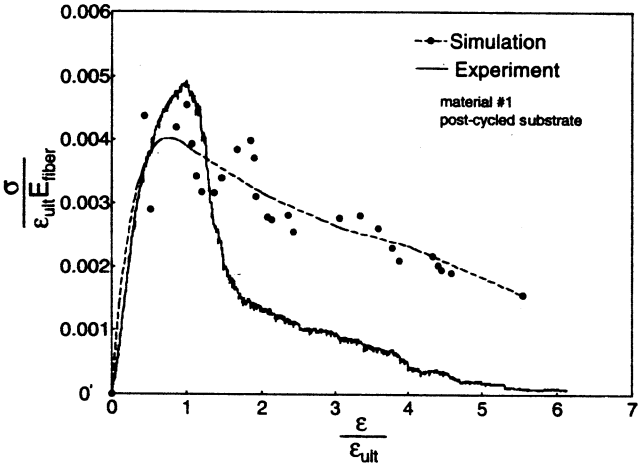

Fig. 7(*b*)

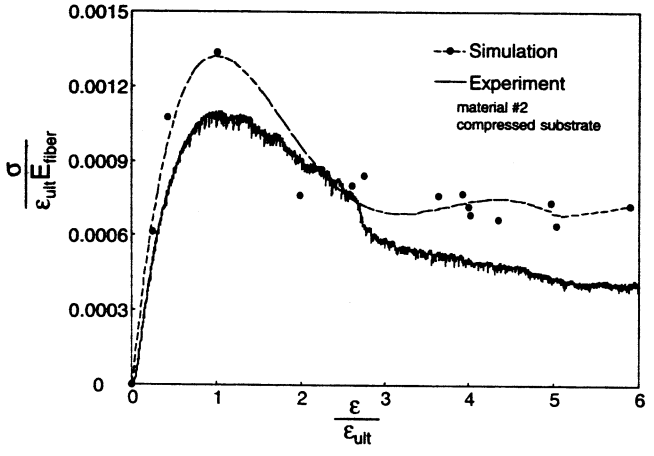

Fig. 7(*c*)

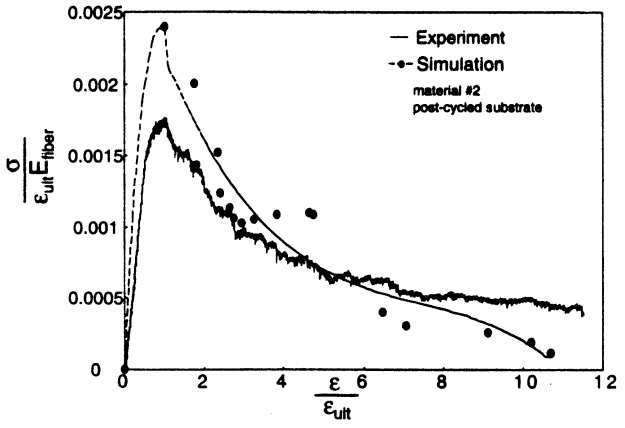

Fig. 7(*d*)

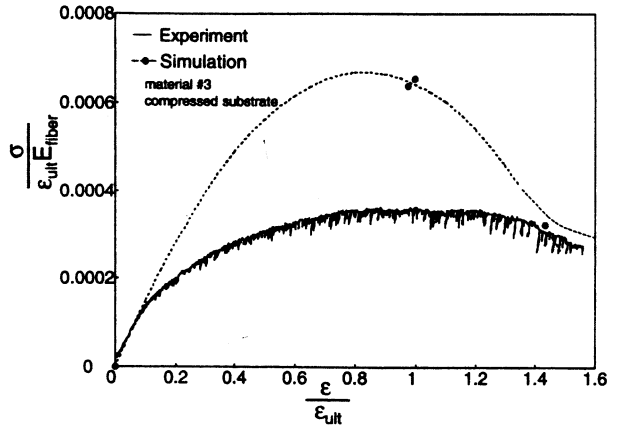

Fig. 7(*e*)

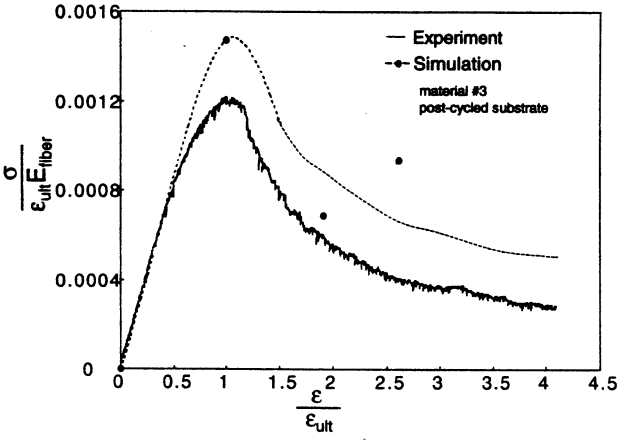

Fig. 7(*f*)

Fig. 7 Simulation stress-strain curves versus experimental curves for representative specimens, in two conditions, each material: compressed to cycling thickness, and post-cycled (40 constant current, 150% overcharge cycles) for (*a*)–(*b*) material #1; (*c*)–(*d*) material #2; and (*e*)–(*f*) material #3. In each case, simulation curves are shown for the higher and lower staple lengths reported by the manufacturer. Higher and lower staple lengths for each material are shown in Tables 1 and 2.

IV Discussion

The network generation technique, in conjunction with the micromechanical models presented here, offer some insight into design and evolution morphology of substrate materials. Corrosion and electrodeposition, which cause changes in substrate architecture (Wang et al., 1999) can be reasonably represented by the methods shown.

Clearly, the classic rigorous bounds on behavior of fibrous media do not provide sufficiently narrow predictions of properties to allow design of substrates. Indeed, the stochastically-arranged networks often fail to "percolate" for the technologically important case of very low volume fraction. Particularly in this regime, variance in both mechanical and transport properties is large, and the average is well below the upper bound. All of these characteristics are correctly captured by the models presented here. However, some mechanics simulations exhibited local areas of

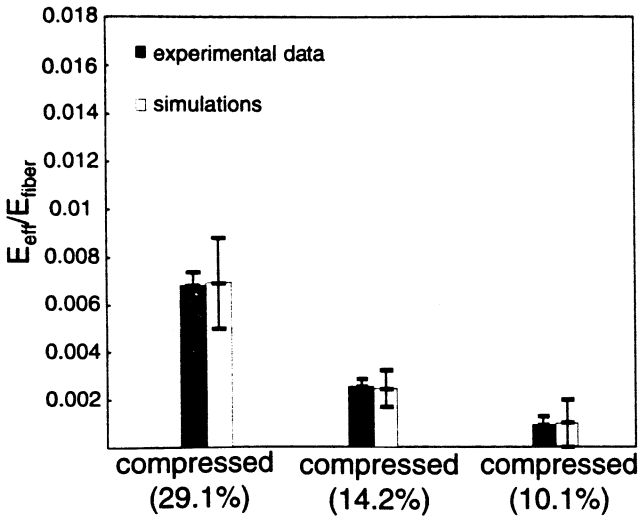

Fig. 8 Simulations versus experimental data, for initial moduli for all materials in the compressed to cycling thickness condition. Torsion spring constants in each case are shown in Table 2.

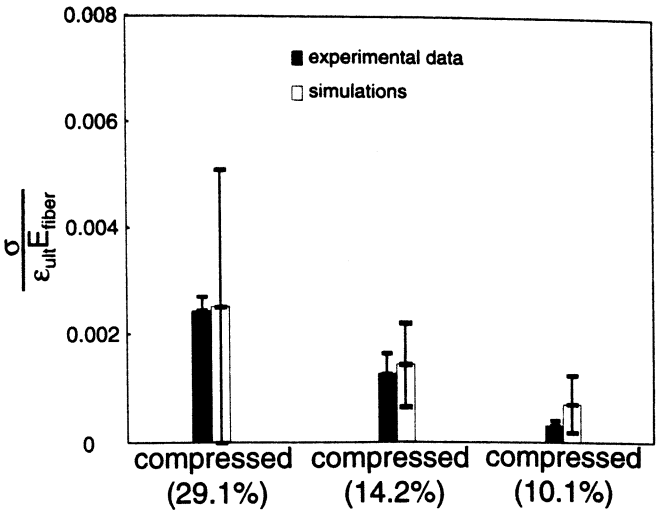

Fig. 10 Simulations versus experimental data, for peak stresses for all materials in the compressed to cycling thickness condition. Torsion spring constants in each case are reported in Table 2.

very large rotations around spring-joined fibers (up to 75 deg). This was observed frequently in areas of very short beams, which occur with greater connectivity (i.e., greater fiber density). Numerical instabilities also arise more commonly in high density, small window-size simulations, and sometimes produce very large local displacements in short beams. This is a subject of ongoing work, to assess the effects of local plasticity on network behavior.

Implications for Design of Substrates. Substrate evolution during cycling must be accounted for in design of materials. Though ideally, compression of cells could eventually be eliminated with improved materials design, it is a commonly-performed step in assuring good transport over cycle life. Thus, material compression must be taken into account in design for conductivity. Also, the consumption and redeposition of particle mass in the cell causes very significant changes in the networks modeled. Doubling of aspect ratios of fibers has important consequences for transport properties—indeed, these morphological changes alone can explain much of the reduction in conductivity measured experimentally. In essence, one must design for minimum conductivity in the post-cycled condition if substrates comprised of mixtures of fibers and particles are to be used. Further corrosion of the substrates is possible in more aggressive cycling conditions and higher cycle experiments. The best strategy in modeling, however, is probably to separate electrodeposition modeling from the network behavior, thus carrying out design in two steps: first, assessing the likely changes in architecture during cycling, and second, modeling the conductivity of the final microstructure to determine minimum requirements on mass of conductor. Simulations here show that the second step can be performed with excellent accuracy guided by experiments.

The mechanical properties and models reported serve as "proof tests" of material evolution; they also address the matter of swelling indirectly. The 2D simulations showed that bond stiffness would have to be quite low in order to explain the observed behavior (note the very small values of k obtained in Table 2), in the absence of plasticity in the model. Experimental evidence suggests very little overall permanent deformation of materials after cycling, motivating the elastic models, but displacements and rotations can be locally high in stochastic systems; these effects are studied in greater detail elsewhere (Wang and Sastry, 1999). The 3D problem of determination of material resistance to failure in transverse planes (i.e., loss of conductivity of the positive plate due

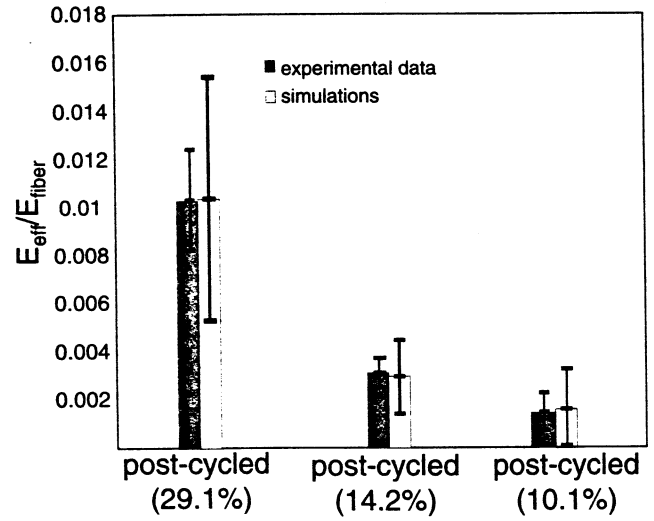

Fig. 9 Simulations versus experimental data, for initial moduli for all materials in the post-cycled (40 constant current, 150% overcharge cycles) condition. Torsion spring constants in each case are shown in Table 2.

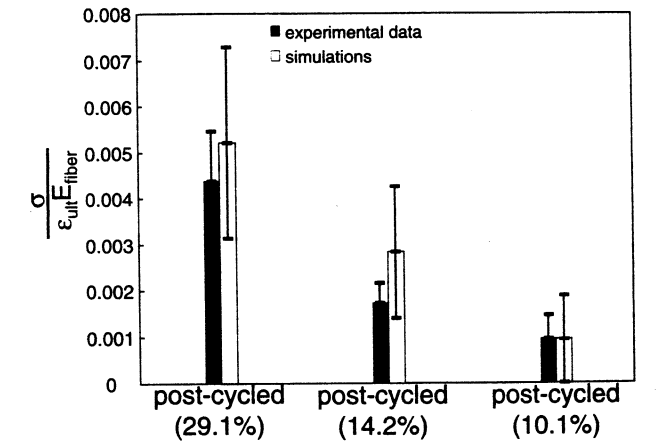

Fig. 11 Simulations versus experimental data, for peak stresses for all materials in the post-cycled (40 constant current, 150% overcharge cycles) condition. Torsion spring constants in each case are reported in Table 2.

to transverse failures, an issue for uncompressed cells), must incorporate observations and simulations of the bond behavior in the plane. It is probably reasonable to assume that bonds behave much the same way, regardless of location, but the long beam sections which span the thickness of the materials would inherently offer much different balances of loads borne in bending, torsion and tension than the shorter beams (note average segment lengths in the 2D sections are small in all cases, Table 2) in the plane of the networks studied, necessitating fully 3D simulations for those materials.

In both 2D and 3D, scale effects in heterogeneous microstructures are critically important. The simulations performed here, however, were at similar scale to the samples studied, offering immediate design insight. Clearly, one would prefer to select the smallest "window size" of simulation possible, relative to characteristic size of microstructure. In transport, because of the connectivity/conduction model adopted, scale effects were quite small (see also Cheng et al., 1999a, b). In essence, contact resistance was ignored as a mechanism (a method validated by here by experiments).

Mechanics Scale and Geometry Effects. In mechanics, by contrast, scale effects were seen to be very important, necessitating simulations at shorter staple lengths. Simulations performed at shorter staple lengths in all cases resulted in higher torsion constants, by as much as nine orders of magnitude. In general, simulations run at long staple lengths, at the scales listed, showed very poor correlation and unrealistic local deformations.

The difference between the compressed and post-cycled network change (amounting to a halving of staple fiber aspect ratio) was significant, but the scale effect dominated. In essence, it was found that for long staple lengths, experimental results were consistent with negligibly small bond stiffnesses. This clearly is not physically realistic, given that the average segment lengths in the short, long and uniformly-distributed staple length cases were approximately equivalent in all cases. Rather, this is a stochastic effect: staple lengths in the neighborhood of the size of the simulation window produced several domain spanning fibers in each case. These spanning fibers, with the tensile stiffness of nickel rather than a much lower effective stiffness resulting from bending and torsion of a series of connected beams, produced these results. This issue is addressed in other ongoing work in greater detail (Wang and Sastry, 1999).

Materials studied were of different volume fraction and material geometry (with material 3, 5% volume fraction as-received, having longer staple lengths than the other two materials). Thus, two interrelated effects were examined through the mechanics simulations:

(1) the effect of aspect ratio on mechanical properties (i.e., post-cycled behavior versus compressed), and
(2) the effect of volume fraction in all cases (three cases were studied).

The effects are discussed in order, with sample networks shown for purpose of illustration in Figs. 12–14.

In the first comparison, we are motivated by a need to develop technologically relevant information about the effect of cycling on substrate properties, in order to design materials which will maintain good conductivity over long cycle lives. Gradual redeposition of nickel in these materials reduces aspect ratio of the constituent fibers. Simulation and experimental results are entirely consistent with the original hypothesis of this work, that this morphological change explains much of the increase in resistivity during cycling. The attendant increase in both stiffness and strength cannot be explained only by this change in aspect ratio, however, since this distribution of mass in lower-aspect ratio materials results in fewer overall fibers, reduced connectivity, and attendant reduction in stiffness (in the case of rigid bonds). If the bonds are modeled as described, a result consistent with evolution of morphology is found; namely, that simultaneous material redeposition on the bonds causes stiffening of the materials' bonds.

In the second question, of the effect of volume fraction, only two materials were actually comparable due to the longer staple lengths used in material three (and the generally high dependence of staple length in all cases). As expected, the higher volume fraction material (material 1, as-received volume fraction 18%; compressed and post-cycled, 29.1%) exhibited greater overall stiffness and strength than and lower resistivity, than the lower volume fraction material (material 2, as-received volume fraction 7%; compressed and post-cycled, 14.2%). While providing superior mechanical properties and conductivities, higher volume fraction materials come at severe weight penalty, thus restricting energy densities—as mentioned in earlier papers, the substrate material can comprise approximately 35% of cell mass in NiMH batteries. Only moderate gains were shown between the 5% and 7% volume fraction materials studied, and therefore the better strategy is probably to increase the fiber staple lengths in networks rather than focusing on moderate increases in conductive mass, or conductivity of other cell materials (see Cheng et al., 1999a, b for more discussion on this point).

V Conclusions and Future Work

Comparisons of micromechanical models and experimental data have produced good agreement for the materials studied. Results point to use of higher aspect ratio fibers for use in substrates, with modeling also necessary to account for structural changes during cycling.

Several numerical issues regarding simulations of deformation in simple beams of widely varying length distribution arose in this work, and are the subject of ongoing study (Wang and Sastry, 1999). Some simulations exhibited local areas of very large rotations around spring-joined fibers. This was observed frequently in areas of very short beams, which occur with greater connectivity (i.e. greater fiber density), but did not result in large axial strains in beam elements. Numerical instabilities arose more commonly in high density, small window-size simulations, sometime producing very large local displacements in short beams. Future work will be focused on the importance of scale of simulation in these cases, to better identify where physically representative problems will necessitate improved numerical approaches.

Future work will address some physical mechanisms that have been approximated in the current studies, including the kinetics of the cell reaction, and contact versus bulk conduction. Additional studies of fiber-particle interaction are also warranted, based on results here. Finally, studies incorporating plasticity and dynamic loads are planned, with some experimental efforts focused on investigation of the changing nature of material bonds over cycle life.

Acknowledgments

This work was supported by the Lawrence Berkeley Laboratories, through the Exploratory Research Program of the U.S. Department of Energy. Additional support and materials were kindly provided by Mr. Robert Hellen and Mr. Tom Kelly, of Yardney Technical Products, Pawcatuck, CT; Ms. Susan Herczeg of National Standard; and Mr. Marshall Muller at Ovonic Battery Company. Support provided by an NSF PECASE grant is also gratefully acknowledged.

References

Alzebdeh, K., and Ostoja-Starzewski, M., 1993, "Micromechanically Based Stochastic Finite Elements," *Finite Element in Analysis and Design*, Vol. 15, pp. 35–41.

Balberg, I., and Binenbaum, N., 1983, "Computer Study of the Percolation Threshold In A Two-Dimensional Anisotropic System of Conducting Sticks," *Physical Review B*, Vol. 29, No. 7, pp. 3799–3812.

Borcea, L., and Papanicolaou, G. C., 1997, "A Hybrid Numerical Method for High Contrast Conductivity Problems," *Journal of Computational and Applied Mathematics*, Vol. 87, pp. 61–77.

Broadbent, S. R., and Hammersley, J. M., 1957, "Percolation Processes: Crystals and Mazes," *Proceedings of the Cambridge Philosophical Society*, Vol. 53, pp. 642–645.

Cheng, X., Sastry, A. M., and Layton, B. E., 1999, "Transport in Stochastic Fibrous Networks," in preparation, ASME JOURNAL OF ENGINEERING MATERIALS AND TECHNOLOGY.

Cheng, X., and Sastry, A. M., 1999, "On Transport In Stochastic, Heterogeneous Fibrous Domains," to appear, *Mechanics of Materials*.

Cox, H. L., 1952, "The Elasticity and Strength of Paper And Other Fibrous Materials," *British Journal of Applied Physics*, Vol. 3, pp. 72–79.

Kirkpatrick, S., 1973, "Percolation And Conduction," *Reviews of Modern Physics*, Vol. 45, No. 4, pp. 574–588.

Hearle, J. W. S., Stevenson, P. J., 1964, "Studies in Nonwoven Fabrics Part IV: Prediction of Tensile Properties," *Textile Research Journal*, Vol. 34, No. 3, pp. 181–191.

Lu, W. T., Carlsson, L. A., and Andersson, Y., 1995, "Micro-model of Paper, Part 1: Bounds on Elastic Properties," *Tappi Journal*, Vol. 78, No. 12, pp. 155–164.

Lu, W. T., and Carlsson, L. A., 1996, "Micro-model of Paper, Part 2: Statistical Analysis of the Paper Structure," *Tappi Journal*, Vol. 79, No. 1, pp. 203–210.

Lu, W. T., and Carlsson, L. A., 1996, "Micro-model of Paper, Part 3: Mosaic Model," *Tappi Journal*, Vol. 79, No. 2, pp. 197–205.

McLachlan, D. S., 1988, "Measurement And Analysis Of A Model Dual-conductivity Medium Using A Generalized Effective-medium Theory," *Journal of Physics C: Solid State Physics*, Vol. 21, pp. 1521–1522.

Pike, G. E., and Seager, C. H., 1974, "Percolation and Conductivity: A Computer Study. I*," *Physical Review B*, Vol. 10, No. 4, pp. 1421–1434.

Oshitani, M., Takayama, T., Takashima, K., and Tsuji, S., 1986, "A Study on the Swelling of Sintered Nickel Hydroxide Electrode," *Journal of Applied Electrochemistry*, Vol. 16, pp. 403–412.

Ostoja-Starzewski, M., and Wang, C., 1989, "Linear Elasticity of Planar Delaunary Networks: Random Field Characterization of Effective Moduli," *Acta Mechanica*, Vol. 80, pp. 61–80.

Ostoja-Starzewski, M., and Wang, C., 1990, "Linear Elasticity Of Planar Delaunary Networks. Part II: Voigt And Reuss Bounds, And Modification For Centroids," *Acta Mechanica*, Vol. 84, pp. 47–61.

Sastry, A. M., 1994, "Modeling Conductivity of Composite Substrates for Nickel-Metal Hydride Batteries," Sandia Report SAND94-2884.

Sastry, A. M., Cheng, X., and Wang, C. W., 1998a, "Mechanics Of Stochastic Fibrous Networks," *Journal of Thermoplastic Composite Materials*, Vol. 11, pp. 288–296.

Sastry, A. M., Cheng, X., and Choi, S. B., 1998b, "Damage in Composite NiMH Positive Electrodes," ASME JOURNAL OF ENGINEERING MATERIALS AND TECHNOLOGY, Vol. 120, pp. 280–283.

Seager, C. H., and Pike, G. E., 1974, "Percolation And Conductivity: A Computer Study, II*," *Physical Review B*, Vol. 10, No. 4, pp. 1435–1446.

USABC, 1996, "USABC Electric Vehicle Battery Test Procedures Manual, Revision 2," principal author: Gary Hunt, Idaho National Engineering Laboratory (INEL), U.S. Department of Energy Idaho Field Office, DOE/ID-10479, Rev. 2.

Wang, C. W., Cheng, X., Sastry, A. M., and Choi, S. B., 1999, "Investigation of Failure Processes in Porous Battery Substrates: Part I—Experimental Findings," ASME JOURNAL OF ENGINEERING MATERIALS AND TECHNOLOGY, published in this issue pp.

Wang, C. W., Sastry, A. M., 1999, "Structure, Mechanics and Failure of Stochastic Fibrous Networks," manuscript in preparation.

United States Postal Service

Statement of Ownership, Management, and Circulation

1. Publication Title	2. Publication Number	3. Filing Date
Transaction of the ASME, Journal of Engineering Materials & Technology	0 9 7 - 6 0 0	10/1/99
4. Issue Frequency	5. Number of Issues Published Annually	6. Annual Subscription Price
Quarterly	Four	$205

7. Complete Mailing Address of Known Office of Publication (Not printer) (Street, city, county, state, and ZIP+4): Three Park Avenue, New York, NY 10016-5990 — Contact Person: Marni Rice; Telephone: (212) 591-7893

8. Complete Mailing Address of Headquarters or General Business Office of Publisher (Not printer): Three Park Avenue, New York, NY 10016-5990

9. Full Names and Complete Mailing Addresses of Publisher, Editor, and Managing Editor (Do not leave blank)

Publisher (Name and complete mailing address): ASME International, Three Park Avenue, New York, NY 10016-5990

Editor (Name and complete mailing address): David L. McDowell GWW School of ME, Georgia Institute of Technology, Atlanta, GA 30332-0405

Managing Editor (Name and complete mailing address): Cornelia Monahan, ASME, Three Park Avenue, New York, NY 10016-5990'

10. Owner (Do not leave blank. If the publication is owned by a corporation, give the name and address of the corporation immediately followed by the names and addresses of all stockholders owning or holding 1 percent or more of the total amount of stock. If not owned by a corporation, give the names and addresses of the individual owners. If owned by a partnership or other unincorporated firm, give its name and address as well as those of each individual owner. If the publication is published by a nonprofit organization, give its name and address.)

Full Name	Complete Mailing Address
ASME International	Three Park Avenue, New York, NY 10016-5990

11. Known Bondholders, Mortgagees, and Other Security Holders Owning or Holding 1 Percent or More of Total Amount of Bonds, Mortgages, or Other Securities. If none, check box → ☐ None

Full Name	Complete Mailing Address

12. Tax Status (For completion by nonprofit organizations authorized to mail at nonprofit rates) (Check one)
The purpose, function, and nonprofit status of this organization and the exempt status for federal income tax purposes:
☒ Has Not Changed During Preceding 12 Months
☐ Has Changed During Preceding 12 Months (Publisher must submit explanation of change with this statement)

PS Form 3526, September 1998 (See Instructions on Reverse)

13. Publication Title: Transaction of the ASME Journal of Engineering Materials & Technology	14. Issue Date for Circulation Data Below: July 1999	
15. Extent and Nature of Circulation	Average No. Copies Each Issue During Preceding 12 Months	No. Copies of Single Issue Published Nearest to Filing Date
a. Total Number of Copies (Net press run)	2086	2071
b. Paid and/or Requested Circulation (1) Paid/Requested Outside-County Mail Subscriptions Stated on Form 3541. (Include advertiser's proof and exchange copies)	906	969
(2) Paid In-County Subscriptions (Include advertiser's proof and exchange copies)	337	102
(3) Sales Through Dealers and Carriers, Street Vendors, Counter Sales, and Other Non-USPS Paid Distribution	287	361
(4) Other Classes Mailed Through the USPS	49	47
c. Total Paid and/or Requested Circulation (Sum of 15b. (1), (2),(3),and (4))	1579	1479
d. Free Distribution by Mail (Samples, complimentary, and other free) (1) Outside-County as Stated on Form 3541		
(2) In-County as Stated on Form 3541		
(3) Other Classes Mailed Through the USPS	32	37
e. Free Distribution Outside the Mail (Carriers or other means)	—	—
f. Total Free Distribution (Sum of 15d. and 15e.)	32	37
g. Total Distribution (Sum of 15c. and 15f)	1611	1516
h. Copies not Distributed	475	555
i. Total (Sum of 15g. and h.)	2086	2071
j. Percent Paid and/or Requested Circulation (15c. divided by 15g. times 100)	98.07	97.6%

16. Publication of Statement of Ownership
☒ Publication required. Will be printed in the October issue of this publication. ☐ Publication not required.

17. Signature and Title of Editor, Publisher, Business Manager, or Owner: Marni Rice — Circulation Coordinator — Date: 10/1/99

I certify that all information furnished on this form is true and complete. I understand that anyone who furnishes false or misleading information on this form or who omits material or information requested on the form may be subject to criminal sanctions (including fines and imprisonment) and/or civil sanctions (including civil penalties).

Instructions to Publishers

1. Complete and file one copy of this form with your postmaster annually on or before October 1. Keep a copy of the completed form for your records.
2. In cases where the stockholder or security holder is a trustee, include in items 10 and 11 the name of the person or corporation for whom the trustee is acting. Also include the names and addresses of individuals who are stockholders who own or hold 1 percent or more of the total amount of bonds, mortgages, or other securities of the publishing corporation. In item 11, if none, check the box. Use blank sheets if more space is required.
3. Be sure to furnish all circulation information called for in item 15. Free circulation must be shown in items 15d, e, and f.
4. Item 15h., Copies not Distributed, must include (1) newsstand copies originally stated on Form 3541, and returned to the publisher, (2) estimated returns from news agents, and (3), copies for office use, leftovers, spoiled, and all other copies not distributed.
5. If the publication had Periodicals authorization as a general or requester publication, this Statement of Ownership, Management, and Circulation must be published; it must be printed in any issue in October or, if the publication is not published during October, the first issue printed after October.
6. In item 16, indicate the date of the issue in which this Statement of Ownership will be published.
7. Item 17 must be signed.

Failure to file or publish a statement of ownership may lead to suspension of Periodicals authorization.

PS Form 3526, September 1998 (Reverse)